DRAFT VERSION AUGUST 27, 2018
Preprint typeset using LaTeX style emulateapj v. 03/07/07

RELATIVISTIC PLASMA AS THE DOMINANT SOURCE OF THE OPTICAL CONTINUUM EMISSION IN THE BROAD-LINE RADIO GALAXY 3C 120

J. LEÓN-TAVARES[1,2,3⋆], A. P. LOBANOV[1], V. H. CHAVUSHYAN[2], T. G. ARSHAKIAN[1], V. T. DOROSHENKO[4,5,6], S. G. SERGEEV [5,6], Y. S. EFIMOV [5,6], AND S.V. NAZAROV[5]

Draft version August 27, 2018

ABSTRACT

We report a relation between radio emission in the inner jet of the Seyfert galaxy 3C 120 and optical continuum emission in this galaxy. Combining the optical variability data with multi-epoch high-resolution very long baseline interferometry observations reveals that an optical flare rises when a superluminal component emerges into the jet and its maxima is related to the passage of such component through the location a stationary feature at a distance of ≈1.3 parsecs from the jet origin. This indicates that a significant fraction of the optical continuum produced in 3C 120 is non-thermal and it can ionize material in a sub-relativistic wind or outflow. We discuss implications of this finding for the ionization and structure of the broad emission line region, as well as for the use of broad emission lines for determining black hole masses in radio-loud AGN.

Subject headings: galaxies: active — galaxies: jets — galaxies: individual (3C 120) — radio continuum: galaxies — acceleration of particles

1. INTRODUCTION

In the current astrophysical paradigm for active galactic nuclei (AGN), each constituent of an AGN contributes to a specific domain in the spectral energy distribution (SED). The SED of some AGN, show a significant amount of energy excess at UV/optical wavelengths, which is commonly attributed to be produced in an accretion disk around the putative central supermassive black hole (BH). Surrounding the accretion disk at $\lesssim 1$ pc, there is a central broad line region (BLR) formed by high density gaseous clouds orbiting the central BH. The thermal UV/optical emission radiated from the disk is thought to be the prime source of variable optical continuum and a dominant factor for the ionization of the BLR material. In radio-loud AGN however, the broad-band continuum can also have a substantial contribution from non-thermal synchrotron radiation generated in the relativistic jet (D'Arcangelo et al. 2007, Marscher et al. 2008, Soldi et al. 2008). To understand the mechanism and properties of the broad-line generation in such objects, it is pivotal to be able to localize and identify the region where the bulk of the non-thermal optical continuum emission is produced.

An efficient way to identify a region responsible for the production of the variable optical continuum emission in radio-loud AGN is to combine long-term optical monitoring and regular very long baseline interferometry (VLBI) observations. A link between the optical emission and relativistic jet in 3C 120 was suggested by Belokon (1987), based on a correlation found between the optical outburst and ejections of plasma clouds (jet components) in the jet. Using the radio and optical data available from 14 years monitoring of the radio galaxy 3C 390.3, Arshakian et al. (2008, 2009) found that ejections of new components can be associated with optical flares occurring on time scales from months to years and reaching their maxima during passages of the jet components through a stationary emitting region in the inner jet, at a distance of ~ 0.5 pc from the jet origin. This indicates that the variable optical continuum emission can be generated in the innermost part of the jet, in the region located upstream from the stationary feature. This has an important implication for the existence of a non-virialized outflowing broad-line region associated with the jet.

It should be noted that stationary and low-pattern speed features have been recently reported in parsec-scale jets of a number of prominent radio sources (*e.g.*, Kellermann et al. 2004, Savolainen et al. 2006, Lister et al. 2009b), alongside faster, superluminally moving components embedded in the same flows (Kellermann et al. 2004, Jorstad et al. 2005). Although specific geometric conditions and extremely small viewing angles may lead to formation of such features in relativistic flows (Alberdi et al. 2000), it is more likely that these features represent standing shocks (for instance, recollimation shocks in an initially over-pressurized outflow; Gómez et al. 1995, Perucho & Martí 2007). Such standing shocks may play a major role in accelerating particles near the base of the jet (Mandal & Chakrabarti 2008; Becker et al. 2008), and could be responsible for the persistent high levels of polarization in blazars (D'Arcangelo et al. 2007; Marscher et al. 2008).

It is important to understand whether the correlations found in Arshakian et al. (2008, 2009) are characteristic only for the 3C 390.3 or common for all radio galaxies and quasars. In this letter, we combined archival VLBI monitoring data and data available from photometric monitoring of 3C 120 to study the link between properties of the superluminal jet and optical continuum flares.

Throughout the paper, a flat ΛCDM cosmology is assumed, with the Hubble constant $H_0 = 70$ km s^{-1} Mpc^{-1} and matter density $\Omega_m = 0.3$. This corresponds to a linear scale of 0.658 pc/mas, at the redshift $z = 0.033$ of 3C 120.

2. OBSERVATIONS

[1] Max-Planck-Institut für Radioastronomie, Auf dem Hügel 69, 53121 Bonn, Germany
[2] Instituto Nacional de Astrofísica Óptica y Electrónica, Apartado Postal 51 y 216, 72000 Puebla, México
[3] Aalto University Metsähovi Radio Observatory, Metsähovintie 114, FIN-02540, Kylmälä, Finland
[4] Crimean Laboratory of the Sternberg Astronomical Institute, P/O Nauchny, Crimea 98409, Ukraine
[5] Crimean Astrophysical Observatory, P/O Nauchny, Crimea 98409, Ukraine
[6] Isaac Newton Institute of Chile, Crimean Branch
⋆ leon@kurp.hut.fi

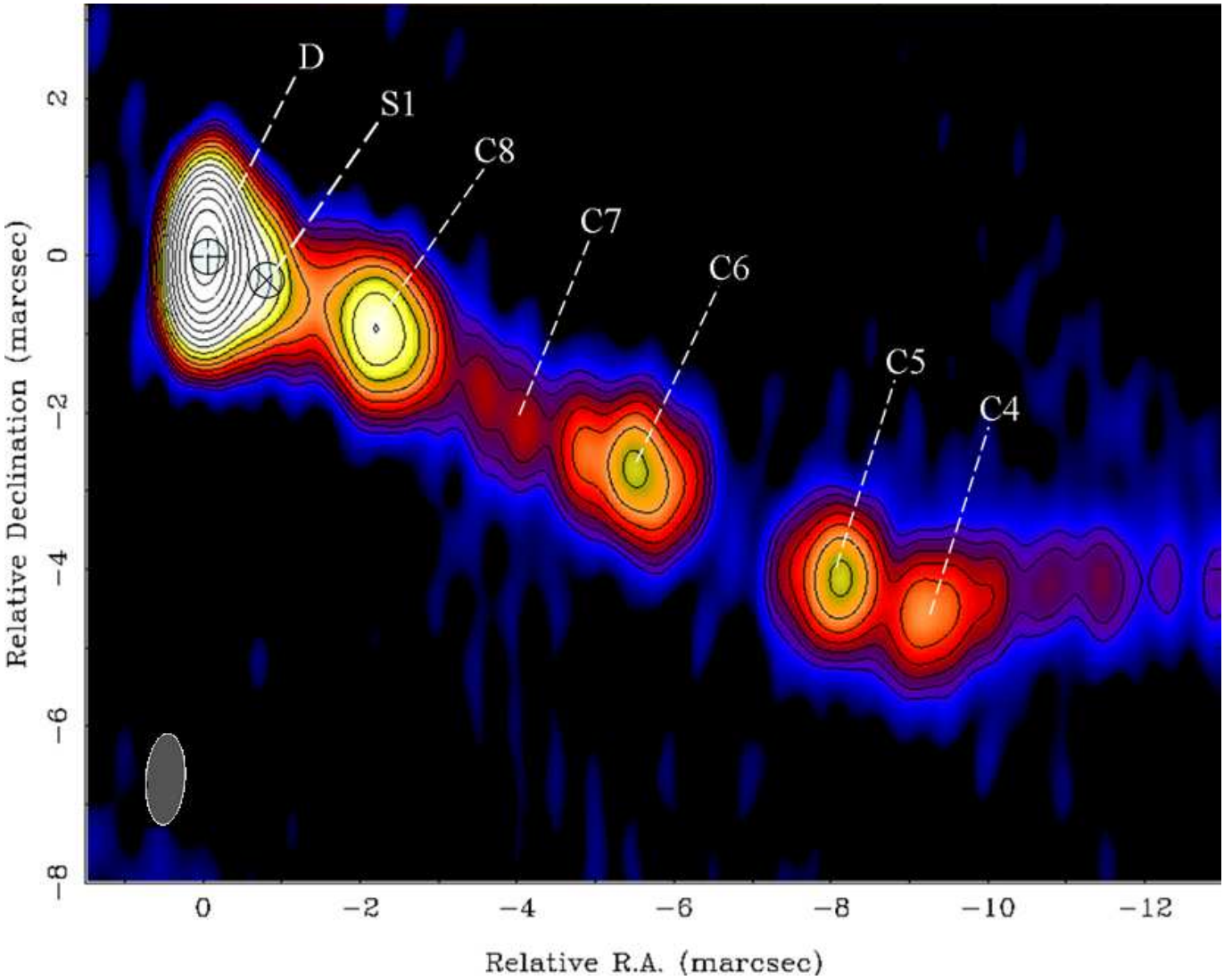

FIG. 1.— Compact jet in 3C 120 observed on January 7, 2005, with the VLBA at 15 GHz (2cm). Shaded ellipse in the lower left corner marks the restoring point-spread function (beam) with the FWHM of 0.53 × 1.26 mas oriented at an angle of three degrees (clockwise rotation). The peak flux density in the image is 974 mJy/beam and the rms noise is 0.26 mJy/beam. Contours are drawn at 1, $\sqrt{2}$, 2...% of the lowest contour shown at 0.9 mJy/beam. The jet structure is parametrized by a set of two-dimensional, circular Gaussian features obtained from fitting the visibility amplitudes and phases (Pearson 1997). The model-fit components (C4-C12) located within the inner 14 mas from the core are shown in Figure 2. Label marks show the location of the model-fit components and the two stationary components D and S1 are highlighted by open circles.

To match the available optical monitoring data, twenty VLBA[8] observations of 3C 120 made between 2001 December 23 and 2008 November 26 have been retrieved from the MOJAVE (Monitoring of Jets in Active Galactic Nuclei) database. Details of the observations and reduction of the MOJAVE data are presented in Kellermann et al. (1998,2004); Lister & Homan (2005); Lister et al. (2009a). Individual images of the VLBA experiments analyzed in this work can be found at the MOJAVE website[9]. VLBI images for all twenty epochs have been produced, applying standard self-calibration and hybrid imaging procedures (cf., Cornwell & Fomalont 1999) to uniformly weighted and untapered visibility data.

The optical CCD-BVRI observations used in this paper were carried out at the 70-cm telescope of the Crimean Astrophysical Observatory from 2002 January 05 to 2008 March 11. The details about instrument, device and observations are described in Sergeev et al. (2005). The CCD camera Ap7p was mounted on the prime focus (f=282 cm) of the telescope. The CCD is provided for B,V,R,R1,I filters, where R1 filter closely resembles the Cousins I filter, while the other filters matches closely to the standard Johnson filters. We used the light curve in B filter, constructed from aperture photometry through a 15" diameter aperture centered on the galaxy nucleus relative to a comparison star No. 1 in the field (Doroshenko et al. 2005).

3. STRUCTURE AND KINEMATICS OF THE JET

The 15 GHz radio structure of 3C 120 shown in Figure 1 is characterized by a one-sided jet directed at a P.A. of about –120°. Two dimensional circular Gaussian components were fitted in the (*u*,*v*)-domain to the fully calibrated visibility data using the modelfitting technique (cf., Pearson 1997).

Robustness of the modelfitting is verified by comparing the noise properties and the peak and total flux densities corresponding to the Gaussian component models to those from

[8] Very Long Baseline Array of the National Radio Astronomy Observatory, USA

[9] http://www.physics.purdue.edu/MOJAVE/sourcepages/0430+052.shtml

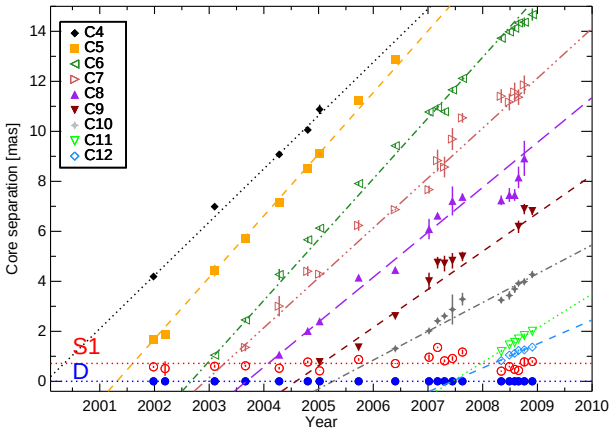

FIG. 2.— Relative separations of the jet components from the stationary feature D (blue circles) for 20 epochs of the VLBA observations of 3C 120. Moving components are denoted by their respective label marks. A stationary component S1 is denoted by red open circles. The lines represent the best linear least-squares fits to the component separations. Errors smaller than symbols may not be visible.

the respective hybrid images. This is done by using the procedure described in the appendix of Arshakian et al. (2009). We find that, in all our model fits, these parameters are similar to those from the respective hybrid images, which indicates that the Gaussian model fits represent adequately the structure of the source.

Self-consistency of the component identification is verified by requiring a smooth kinematic and flux density evolution of each of the individual components, similarly to the methods employed in other works dealing with long-term VLBI monitoring data (cf., Lobanov 1996, Lobanov & Zensus 1999). We restrict our analysis to a full kinematic model for the inner 14 milliarcseconds (mas) of the jet, since beyond that distance a reliable model could not be established due to the lower surface brightness and high complexity of the outer region. We identify nine moving features (C4-C12) moving down the jet at superluminal speeds. Estimates of errors of the integrated flux density, size and position of each component in the inner jet were calculated using the method given by Fomalont (1999), taking into account the resolution limits of the observations (Lobanov 2005).

In all twenty epochs, we identify a stationary component (S1) separated from D by 0.715 ± 0.253 mas, corresponding to the projected linear separation of 0.471 ± 0.133 pc. Adopting an angle of 20.5° (Jorstad et al. 2005) between the jet axis and the line of sight, the corresponding de-projected distance between D and S1 is $\sim 1.35 \pm 0.38$ pc.

Fidelity of the position and flux density measurements for stationary component S1 is verified by comparing them with the resolution limits calculated from the SNR of the detections (see Lobanov 2005, Arshakian et al 2010 for details of the procedure). We find that the component S1 is always resolved and the flux densities of the component D and S1 estimated from the modelfits are uncorrelated, implying that D and S1 are two independent features in the jet.

The apparent positional variations of S1 around its average location can be explained by a combination of variable optical depth of the inner part of the jet (represented by the core component D) and by blending between D and S1 and between S1 and moving jet features. The magnitude of the positional change of the optically thick core D can be estimated

TABLE 1
3C 120 JET COMPONENTS PROPERTIES AND PARAMETERS OF ASSOCIATED OPTICAL FLARES

Component (1)	t_D [yr] (2)	t_{S1} [yr] (3)	β_{app} [c] (4)	t_{fl} [yr] (5)	N_{rel} (6)	τ_{fl} [yr] (7)
C4	2000.02	2000.35	4.56 ± 0.06	...	...	...
C5	2001.31	2001.60	5.26 ± 0.02	<2001.9	<10	>0.1
C6	2002.67	2002.96	5.19 ± 0.01	2002.99	3.10	0.18
C7	2002.94	2003.30	4.28 ± 0.07	2003.21	1.80	0.11
C8	2003.68	2004.08	3.83 ± 0.03	2004.02	1.88	0.10
C9	2004.58	2005.05	3.22 ± 0.06	2005.02	2.52	0.07
C10	2005.26	2005.88	2.46 ± 0.03	2005.85	3.24	0.14
C11	2007.51	2008.00	3.12 ± 0.10	2007.84	4.34	0.22
C12	2007.43	2008.18	2.03 ± 0.08	2008.10	6.66	0.16

NOTE. — Column. (1): Component identifier; Column. (2): t_D - time of ejection from the component D; Column. (3): t_{S1} - time of passage through the stationary component S1; Column. (4): β_{app} radial speed in units of the speed of light; Column. (5): t_{fl} - fitted peak epoch of optical flares associated with individual jet components; Column. (6): N_{rel} - relative particle density increase during a flare; Column. (7): τ_{fl} - characteristic time scale of a flare.

from the core shift of ≈ 1 mas measured between 2.3 GHz and 8.4 GHz (Kovalev et al. 2008) and assuming that the opacity is caused by synchrotron self-absorption (cf. Königl 1981, Lobanov 1998). In this case, the location of the core D would vary $\propto S_D^{2/3}$ and for the flux variability measured in our data at 15 GHz this would result in positional variations with an r.m.s of ≈ 0.2 mas. Since the location of the component S1 is always measured with respect to the component D, this positional variability is attributed to variations of the position of S1. The magnitude of positional uncertainty due to blending can be estimated from the component modelfits following Lobanov (2005) and Arshakian et al. (2010). For the case of blending between D and S1, we estimate an uncertainty of about 0.06 mas. Thus, the nuclear opacity and D-S1 blending alone account for a positional uncertainty of ≈ 0.21 mas, which is close to the measured one. The magnitude of positional uncertainty due to blending between S1 and moving features is difficult to estimate, but we expect that it should be similar or even even larger that the uncertainty due to the D-S1 blending. We therefore conclude that S1 is indeed likely to be a stationary formation inside the relativistic flow in 3C 120.

Time evolution of angular separations of moving jet components from the stationary core (D) is shown in Figure 2. We fitted the component separation by linear regressions and used back-extrapolation of the linear fits to the component separations to calculate apparent speeds, epochs of ejection from the component D (t_D) and epochs of passage through the stationary feature S1 (t_{S1}), for each moving component. The resulting apparent speeds (in units of the sped of light, c), ejection times and times of passages through the stationary component S1 are presented in columns (2)-(4) of Table 1. The linear fits to the observed separations of the components C4-C12 from the component D yield proper motions in the range of 0.9-2.4 mas/yr, which correspond to apparent speeds of 2.0-5.3 c.

4. RELATION BETWEEN THE JET AND THE OPTICAL CONTINUUM

Relation between the radio and optical emission in 3C 120 is presented in Figure 3. In this plot, variations of the optical B-band continuum and radio flux densities of the stationary features D and S1 at 15 GHz are compared to the ejection epochs and epochs of passages of the moving components through the region S1. The optical light curve shows several flares superimposed on a long-term trend. The sparser ra-

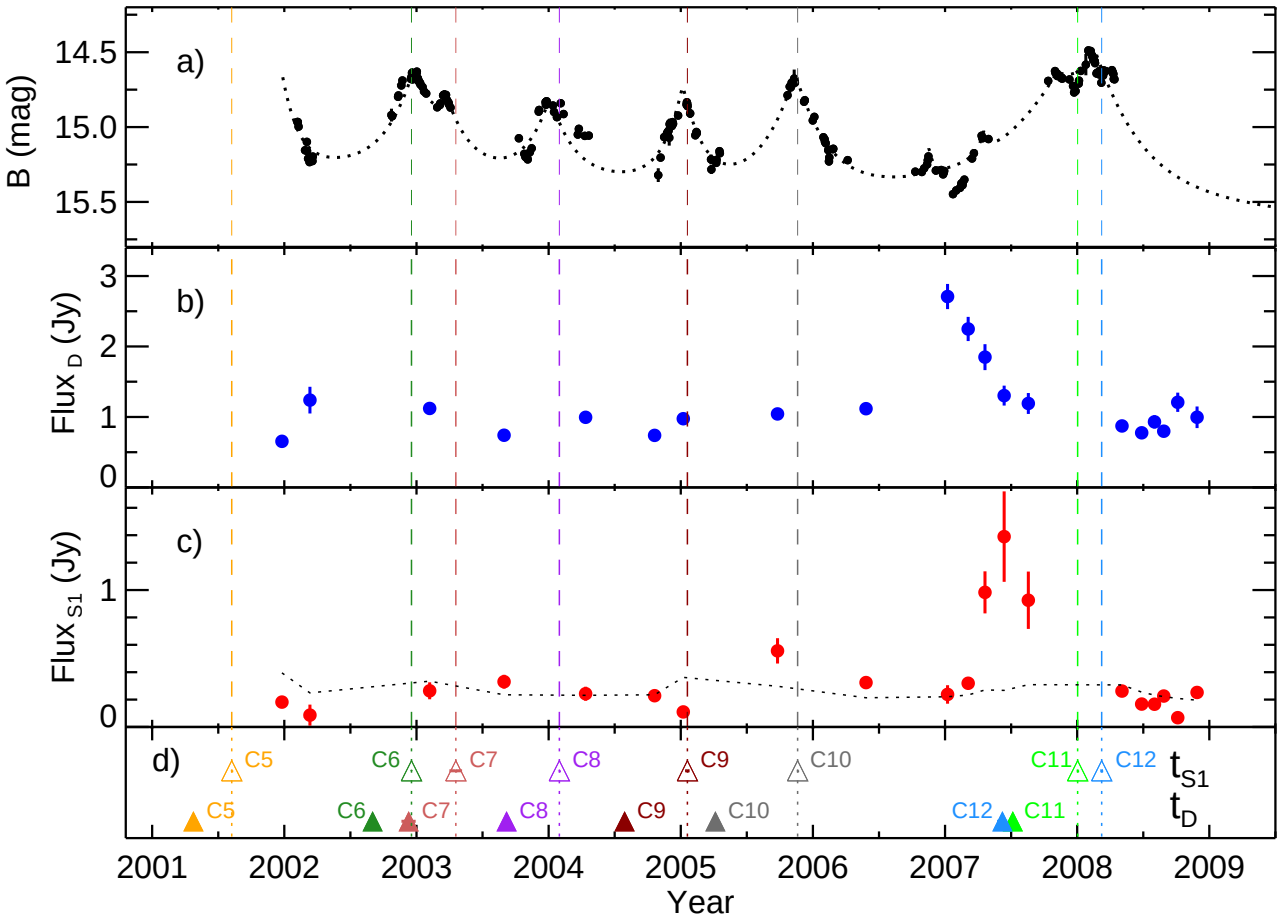

FIG. 3.— Variability of the optical and radio emission and jet kinematics in 3C 120 from 2002 to 2008. Panel description: a) optical B magnitudes (circles) and flare model (dotted line) for the optical variations; b) and c) radio flux densities of the stationary features D and S1 at 15 GHz (dotted line shows flux density changes predicted from the model for the optical flares); d) times of ejection of radio components at D (filled triangles) and times of passages of the moving jet components through S1 (open triangles). The mean time required for the components C4-C12 to move the distance from D to S1 is 0.45 ± 0.14 yr. Each of the seven flares in the optical light curve is correlated with a passage of one of the moving jet features C6–C12 through the location of S1, with an average time delay less than 0.1 yr between the optical and radio events.

dio measurements sample clearly only one strong flare event around 2007, which is visible in the light curves of both D and S1. The epochs of each superluminal ejection (t_D) and passing through the stationary component S1 (t_{S1}) are marked in Figure 3 by filled and open triangles, respectively.

Following an ejection from the jet origin at the region D, it takes a moving jet component 0.45 ± 0.14 years to travel the distance between D and S1. Passages of moving jet components C6-C12 through the region S1 are correlated with local peaks in the optical light curve. The radio passages of new components through S1 lag the maxima of optical flares by an average delay < 0.1 yr. Application of a statistical test described in Marscher et al. (2002) yields a probability of $\sim 10^{-9}$ for all 7 radio and optical continuum events to be so close in the time by chance. However, there is the possibility that jet components C6-C7 and C11-C12 belong to the same event, respectively. Thus, the probability that 5 passing times would be observed to occur randomly within 0.2 yr of the maxima in the optical flares is $\sim 10^{-5}$. Hence, the correspondence between t_{S1} and maxima of optical flares is still real at a high confidence level. This suggests that the region responsible of optical flares and the stationary component S1 must be physically connected, similarly to the situation in the radio galaxy 3C 390.3 (Arshakian et al. 2009).

We model the optical light curve as synchrotron flares caused by density variations in the relativistic flows, using the approach described in Lobanov & Zensus (1999). We set a quiescent particle density $N_0 = 1$ (as only relative changes of the density are required for the modelling) and estimate a quiescent magnetic field strength $B_0 \approx 0.5$ G from broad band spectral fits (Tyul'bashev & Chernikov 2004). We model the optical variations by density variations with characteristic exponential rise and decay times τ_{fl}. The resulting light curve is shown in Fig. 3 and the flare parameters are presented in Table 1 for the events coinciding with the jet component passages through the region S1. All of the optical flares require a factor of ≤ 7 increase of the particle density, which is physically plausible. For a spectral index $\alpha = -0.5$ of the synchrotron emission, the optical flare fit also yields good predictions for the radio flux density of S1, with an average ratio of 1.2 between the predicted and measured flux densities, given the fact that the radio data have not been used at all for producing the fit. This supports further the suggestions that the optical flares are related to synchrotron emission originated in the vicinity of the stationary feature S1. In 2006.5-2007.5, the optical light curve shows two minor events peaking close to

the peaks of radio emission in D and S1. Our optical fit indicates that the particle density increase during these events is very small, offering a speculation that these flares may result from changes in the magnetic field or Lorentz factor of the jet plasma.

The strong flare detected in the radio in 2007 is likely related to the ejection of two moving components, C11 and C12, following an unusually long period of relative quiescence. The components C6 and C7 may also be related to a single event in the nucleus. Paired ejections of superluminal features have been seen previously in 3C120 (Gómez et al. 2001) and attributed to trailing shocks in the jet. The flux density of D component increased almost by a factor of three during this flare. The flux density of S1 component reacted to the flare in the component D with a time delay of ~ 0.4 years, which is similar to the travel time of the jet features moving from D to S1. However, the components C11 and C12 were ejected at the time when the flare in component D was already fading and the flux density in component S1 reaches the maximum. This peculiarity may reflect specific physical conditions in the jet. It may suggest, for instance that the jet is initially dominated by Poynting flux, and plasma in the moving features is accelerated by conversion of the Poynting flux into particle energy, which occurs downstream from the Poynting flux dominated region. Unfortunately, the present VLBI data are too sparse to uncover such a degree of detail about the physics of the region between the features D and S1, and it is not possible to verify whether the radio flux density of S1 responded to the passage of moving features in the same fashion as the optical continuum. A detailed radio-optical study of a single event in 3C 120 (or a similar object) would be extremely useful for uncovering the complete physical picture of flaring activity.

5. DISCUSSION

The relation between the optical variability and the structural changes of radio emission in 3C 120 indicate that a reliable physical identification of the stationary features D and S1 in the compact jet with respect to the central black hole of 3C 120 is instrumental for understanding the radiation mechanisms and the structure of the region where the bulk of variable continuum emission is produced. The correlations presented above suggest the component D is located at the base of the relativistic jet, while S1 is most likely a recollimation shock or internal oblique shock formed in the continuous relativistic flow (cf., Daly & Marscher 1988, Gómez et al. 1995, Romanova & Lovelace 1996, Marscher et al. 2002, 2008). Alternatively, the component D could be the core of the jet located at some distance from the accretion disk while the component S1 can be identified with a standing shock. Another possibility is that the components D and S1 may be constituting the bases of the counterjet and the jet respectively. In this case, the component S1, located on the jet side, should be brighter than the component D because of the relativistic Doppler effect. It is evident from Figure 3 however that D was the brighter feature over the entire period of the VLBI monitoring. This counter-jet nature of D is further rejected by the later rise of the flux density of S1 during the flare in 2007 – while S1 should have flared before the component D, if the latter was located on the counter-jet side.

These findings should also be discussed in the context of relations between the optical and X-ray emission in 3C 120 reported recently (Kataoka et al. 2007, Marshall et al. 2009, Chatterjee et al. 2009, Doroshenko et al. 2009).

Kataoka et al. (2007) argued that the strength of the narrow Fe Kα indicates that a major fraction of the X-ray emission originates from an unbeamed source, presumably the accretion disk. This conclusion agrees well with our findings, as our correlations result from a flaring component in the jet, which carries about 25% of the total flux density both in the optical and X-ray regimes. This is similar to the what is found for 3C 390.3 (Arshakian et al. 2009) and 3C 345 (Schinzel et al. 2010). In the latter case, the Γ-ray flux density shows a long-term trend similar to a trend in the radio flux density of the compact core, while a (short-term) Γ-ray flare can be related to a similar flare in a stationary feature in the radio jet, also coinciding with a passage of a newly ejected moving jet component. All these results suggest that the flaring component of the X-ray, optical and radio emission is different in its nature from the underlying, quiescent emission associated with the accretion disk, and that it may indeed be produced by a relativistically moving material in the jet.

Marshall et al. (2009) found a correlation found in 3C 120 between the X-ray and optical emission, where X-ray variations were leading the optical ones by approximately 25 days over a period of almost three years. Chatterjee et al. (2009) report an even smaller time delay (0.5 ± 0.4 days) between the X-ray and optical flares. Doroshenko et al. (2009) have used optical photometry and X-ray light curves of 3C 120 over a period of almost 12 years and found different degrees of correlation between the optical and X-ray variations present at different periods in the light curves. The sign of the correlation also depends on the epoch. All these findings indicate that the flaring optical and X-ray emission are produced essentially in the same spatial region. The results of our present work further support this conclusion and enable identifying the location of the production site of the flaring component more accurately, placing it in the relativistic jet, at a ~ 1.3 pc distance from the central black hole of the AGN.

Dips in the X-ray lightcurve of 3C 120 are reported to be followed by appearances of new superluminal components (Marscher et al. 2002, Chatterjee et al. 2009). Chatterjee et al. (2009) have also used 43 GHz VLBI observations and decomposed the 37 GHz light curve of 3C 120 into a sequence of exponential flares, in order to connect the X-ray variations to structural and emission changes in the radio regime.

Chatterjee et al. (2009) identified 14 moving jet components, during the time period of 2002-2007, and do not report a feature that can be considered a direct counterpart of our stationary feature S1. It should be noted that the 43 GHz VLBI observations probe a region of ~ 1 mas in extent, which is comparable to the distance between D and S1 measured at 15 GHz. If the core shift (Königl 1981) between 15 and 43 GHz taken into account (following Lobanov 1998, a shift of 0.1–0.2 mas can be inferred both from an estimate of synchrotron luminosity of ~ 2–5×10^{43} erg/s for the compact core, and from a core shift of 0.9–1.1 mas measured between 2.3 and 8.4 GHz by Kovalev et al. 2008), S1 is likely to locate close to the outer edge of the 43 GHz emission detected by Chatterjee et al. (2009). In this case, its stationarity would be difficult to be recognized from the 43 GHz data, particularly in presence of subsequent ejections of moving jet components. More detailed and high-dynamic range multi-frequency VLBI observations would be needed in order to make a better assessment of the physical conditions in the flow at distances of about 1 mas from the 43 GHz core of the jet.

The overall complexity of the light curves and the jet structure may lead to difficulties of cross-identifying individual

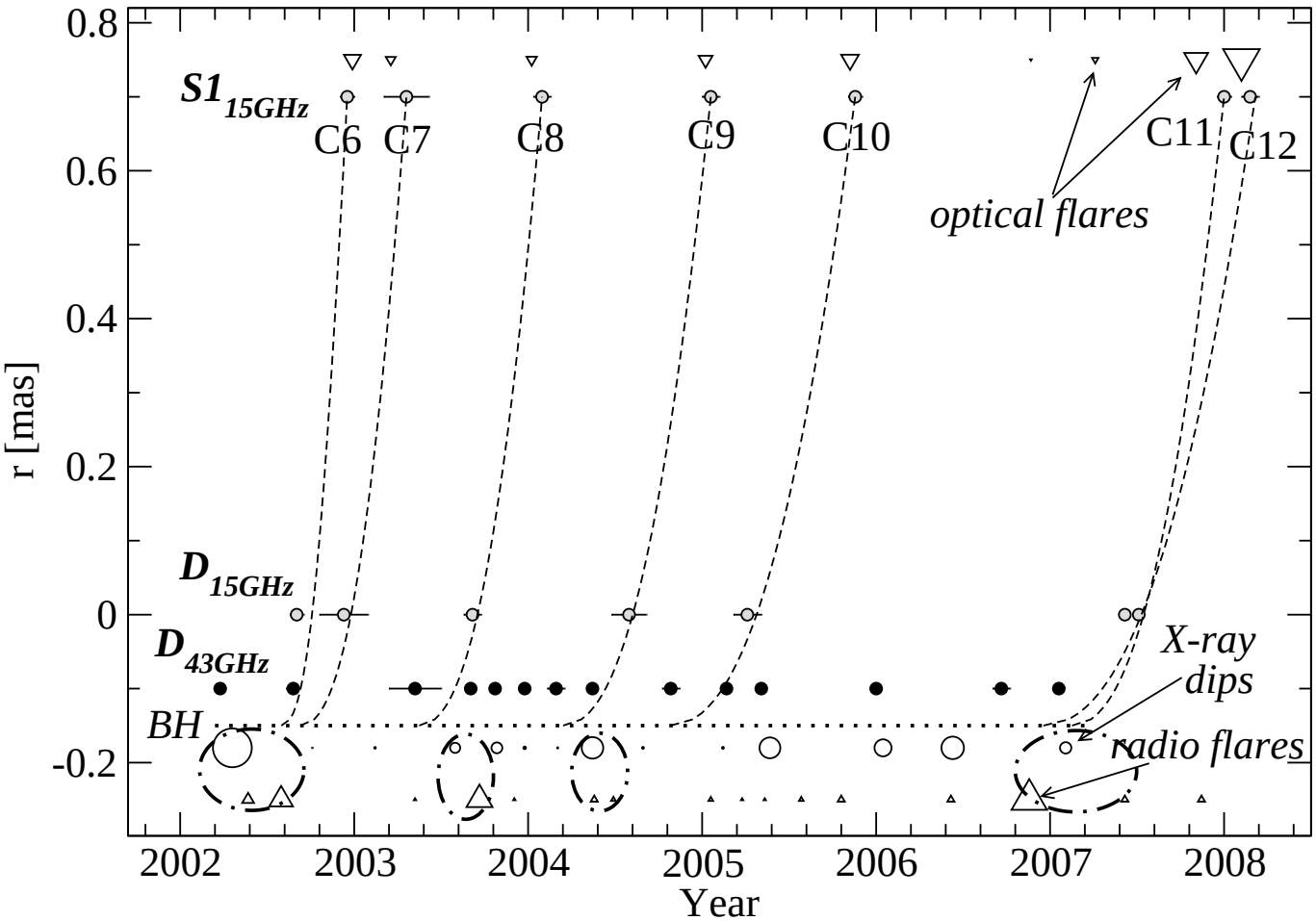

FIG. 4.— Jet kinematics and flaring activity in 3C 120. Black circles (D_{43GHz}) show the ejection epochs of the jet components identified at 43 GHz (Chatterjee et al. 2009). Grey circles show the epochs of ejection (D_{15GHz}) and passages through S1 ($S1_{15GHz}$) of the jet components identified at 15 GHz (this paper). The dotted line indicates the estimated location of the central black hole (BH). Epochs of the X-ray dips (open circles) and 37 GHz radio flares (upward triangles) from Chatterjee et al. (2009) and epochs of the optical flares (downward triangles) are also shown. The apparent angular separation between D_{15GHz} and $S1_{15GHz}$ is measured from the 15 GHz VLBI images. The locations of the core at 43 GHz (D_{43GHz}) and the central black hole are estimated from the core shift as inferred from the synchrotron luminosity of the nuclear jet. Dashed lines show evolution of the component separations obtained using the hydrodynamical acceleration model of Vlahakis and Königl (2004). Dot-dashed ellipses mark possible associations of the 15 GHz components with the X-ray dips and 37 GHz flares.

events in different bands. For instance, three radio flares and two jet identified in Chatterjee et al. (2009) do not have respective counterparts. The relative magnitude of different radio flares, X-ray dips, and brightness of the jet components observed at 43 GHz (*e.g.*, components 04C and 06A) vary by a factor of $\sim 30-60$, with the weaker events and jet components often being difficult to cross-identify. It is possible that the weakest flares and X-ray deeps results from transitory or localised events that do not have a long lasting effect on the jet and cannot be traced at large distances. These weaker jet components can, for example, be destroyed during their passages through the standing shock in S1, and only the strongest components will propagate through and be detected at large distances at 15 GHz.

Based on the considerations above, we attempt now to combine our results with the results from Chatterjee et al. (2009) and to discuss a scheme that could provide a common framework for the entire observational data.

Comparison of the peaks of 37 GHz flares (listed in Table 2 in Chatterjee et al. 2009) and the peaks of the optical flares from our B-band light curve (see Table 1) yields a time delay of 0.43 ± 0.14 yrs, with the radio flares leading the optical flares (epochs of the radio and optical peaks are shown in Figure 4 with upward and downward triangles, respectively). We compute the probability that the 37 GHz peaks shifted by 0.45 yr would be observed to occur randomly within 0.15 yr of the peaks of the optical flares. The probability that 10 out of 16 shifted peaks of 37 GHz flares coincide by chance with the optical peaks is $< 10^{-9}$. It should also be noted that the 37 GHz flares that do not have optical counterparts, are largely located in the seasonal gaps of the optical light curve.

The time lag between the radio and optical flares (where radio is leading) is similar to the time taking a moving component of the jet to travel the distance between D and S1 (0.45 ± 0.14 yrs). Such a succession of the observed flares cannot be easily reconciled with the overall picture of the shock-in-jet model (Marscher and Gear 1985) where the flare propagates from higher to lower frequencies as a shock moves downstream in the jet. One can however attempt to explain such a behavior by a strong acceleration of the emitting material while it travels towards S1 (since the peaks of the optical flares are correlated with the passages of the moving jet components through S1). We combine together the ejection epochs at 15 and 43 GHz and the epochs of component passages through S1 (Figure 4) and plot them together with the times of X-ray dips, and flares in the radio and optical emission. We apply a 0.1 mas core shift between 15 and 43 GHz and use this shift to estimate the central black hole to be lo-

cated at 0.05 mas further upstream from the core at 43 GHz (following Lobanov 1998).

Assuming that the jet accelerates hydrodynamically (*cf.* Vlahakis & Königl 2004) and reaches its terminal speed (characterized by a Lorentz factor $\Gamma_{\rm max}$) at the location of S1, so that $\Gamma_{\rm max}$ can be then inferred for each component from its apparent proper motion (for the adopted value of 20.5° for the jet viewing angle). We apply the description of Vlahakis & Königl, yielding an approximation $\Gamma_{\rm j}(r) = 1+(\Gamma_{\rm max}-1)[r/(r+r_0)]^a$ for the material travelling along the innermost magnetic field line (assumed to originate from the accretion disk at a distance $\varpi \approx 10$ Schwarzschild radii from the central black hole). We find that a characteristic acceleration distance $r_0 = 1.5$ pc (resulting from $\varpi \approx 10^{-4}$ pc) and power index $a = 1$ provide a plausible representation for the evolution of component separations in the acceleration zone between the base of the jet and S1. The resulting model separations are plotted with dashed lines in Figure 4, calculated backwards in time starting from the epochs of component passages through S1. Note that the model curves do not go through the ejection points, $D_{\rm 15GHz}$, as they represent accelerated motions, while the ejection epochs are calculated from linear fits implying a constant speed.

Within this scenario, ejections of all 15 GHz components except C10 can be associated tentatively with strong X-ray dips (circles in Figure 4) and strong radio flares at 37 GHz (upward triangles). It should be further noted that establishing a firm association of this sort requires a detailed knowledge of the component trajectories between D and S1, which could be obtained from a dedicated VLBI monitoring program. The stronger optical flares (downward triangles) are well correlated with the component passages through S1. It should be noted that the terminal speeds for C11 and C12 are poorly constrained, owing to small number of measurements available for these components, and it is feasible that their model ejection epochs may be moved to earlier times. It is not easy to establish a correspondence with the 43 GHz ejection epochs, but it should be possible if the trajectories of 43 GHz components are measured accurately up to a distance of 1 mas from the core and epochs at which they reach this distance are compared with the epochs of passages of the 15 GHz components through the region S1. It is important to verify if the 43 GHz VLBA data reveal any evidence for accelerated motions at distances ≤ 1 mas, which will constrain the physical conditions at sub-milliarcsecond scales.

Based on the discussion above, we can suggest that the 15 GHz components may correspond to the strongest nuclear events, while some of the 43 GHz components may not survive a passage through a standing shock in the jet at the location of the stationary feature S1. The source of the continuum emission is localized not only in the accretion disk (at the extreme vicinity of the black hole) but also in the entire acceleration zone of the jet, with strong flares happening both near the central black hole at D (assumed base of the jet) and at the standing shock (S1) in the jet. This possibility makes 3C 120 one of the prime candidates for studies of flow acceleration and continuum emission production in radio-loud AGN. Clearly, a more general and systematic study of relation between the radio, optical and X-ray emission in 3C 120 is strongly justified.

The correlation between the optical flares and the passages of moving jet components through the location of the stationary feature S1 is best interpreted in terms of disturbances (plasma condensations) propagating in the relativistic flow (Arshakian et al. 2009). In this scenario, the optical continuum generated in 3C 120 is dominated by non-thermal, Doppler-boosted synchrotron emission from a relativistically accelerated plasma in the jet. The jet can be collimated and accelerated on scales of 10^5–$10^6\,R_{\rm g}$ (where $R_{\rm g}$ is the gravitational radius of the central black hole) by an MHD mechanism (e.g. Vlahakis & Königl 2004), with emission peaking at the optical wavelength during a passage through a standing shock compressing the moving material and enhancing substantially the magnetic field. As a moving plasma condensation separates from the standing shock, it appears as a moving knot in the flow. From stellar velocity dispersion measurements of 3C 120 optical spectra, the BH mass is estimated to be $\sim 3.5\times10^7$ M$_\odot$ (Greene & Ho 2006). Thus, the distance of component S1 from the core of the jet corresponds to $\sim 9\times10^5$ $R_{\rm g}$. This scale is consistent with the end of the acceleration and collimation zone in relativistic jets. Further studies, in close detail, of the evolution of compact radio emission during radio and optical flares in objects like 3C 120 is essential for understanding the mechanism for acceleration and energy release in powerful relativistic jets and its relation to generation of non-thermal optical continuum and broad line emission in radio-loud AGN.

6. CONCLUSIONS

To investigate the link between optical continuum variability and subparsec-scale jet in the radio-loud galaxy 3C 120, we combined the radio VLBI (15 GHz) and optical photometry (B-band) data observed during the period of nearly eight years. We found a significant correlation between the jet kinematics on parsec-scales and optical flares on scales from several months to about two years. All optical flares are associated with the jet ejection events: the flare rises after the epoch of ejection of a new jet component (at D) and it reaches the maximum around the epoch at which the ejected radio knot passes the stationary radio component (S1) downstream the jet. The radio passages of new components through S1 delay the maxima of optical flares on the average by $\lesssim 0.1$ yr. These results confirm correlations found in Arshakian et al. (2008, 2009) for the radio galaxy 3C 390.3 and support the idea that the correlation between optical flares and kinematics of the jet could be a common feature for all radio-loud galaxies and quasars.

The link between optical continuum variability and kinematics of the parsec-scale jet is interpreted in terms of optical flares generated by disturbances in the jet flow while moving from the stationary component D of the jet to the stationary component S1 located at a distance of about one parsec. Modeling of optical flares as synchrotron flares caused by density variations in the relativistic flow showed that all optical flares require at most a factor of seven increase of the particle density. The variation of the particle density at subparsec-scales should be smaller if consider a more realistic model in which the magnetic field and/or Lorentz factor of the jet increase downstream of the jet, in the acceleration/collimation zone, between D and S1. In this scenario, the correlated X-ray and optical continuum emission are produced in the relativistic jet at some distance (< 1 pc) from the central black hole rather than in the accretion disk.

Establishing such a relation may have strong implications for the physics of the central regions in radio-loud AGN and AGN in general (see also Arshakian et al. 2009). The link between the optical continuum and radio jet challenges the

existing models in which the optical continuum and broad-line emission are both localized around the disk or near the central black hole of an AGN. It also questions the common assumptions about the central engine used, in particular, for the reverberation mapping technique (Peterson et al. 2002), which combines the broad emission line width with the size of the line-emitting region estimated from the optical continuum luminosity. In 3C 120, a substantial fraction of the ionizing continuum is produced in the relativistic jet and it illuminates thermal material most likely organized in a sub-relativistic outflow. The time delays and profile widths measured in radio-loud AGN may reflect not only the Keplerian motion of the emitting line gas, but also an outflowing component of the gas accelerated by non-gravitational forces. This can lead to large errors in estimates of black hole masses made from monitoring of the broad emission lines.

In order to address these issues, we are carrying out a long-term spectropolarimetry campaign for the 3C 120 and several other nearby radio galaxies aimed to determine the amount of non-thermal optical continuum and to tackle evidence for non-virial motions in the BLR. Follow-up high resolution radio observations at other frequencies and epochs, can help to characterize the nature of the components D and S1.

We thank anonymous referees for a number of useful comments and suggestions which significantly improved this manuscript. This work was supported by CONACYT research grant 54480 (Mexico) and the Russian Foundation for Basic Research (Grant No. 09-02-01136a) . JLT acknowledges support from the CONACYT program for PhD studies, the International Max-Planck Research School for Radio and Infrared Astronomy at the Universities of Bonn and Cologne and the Deutscher Akademischer Austausch Dienst (DAAD) for a short-term scholarship in Germany. This research has made use of data from the MOJAVE database that is maintained by the MOJAVE team (Lister et al. 2009a). The VLBA is an instrument of the National Radio Astronomy Observatory, a facility of the National Science Foundation operated under cooperative agreement by Associated Universities, Inc.

REFERENCES

Alberdi, A., Gómez, J. L., Marcaide, J. M., Marscher, A. P., Pérez-Torres, M. A. 2000, A&A, 361, 529
Arshakian, T. G., León-Tavares, J., Lobanov, A. P., Chavushyan, V. H., Shapovalova, A. I., Burenkov, A. N., & Zensus, J. A. 2010, MNRAS, 401, 1231
Arshakian, T. G., Lobanov, A. P., Chavushyan, V. H., Shapovalova, A. I., & Zensus, J. A. 2008, Relativistic Astrophysics Legacy and Cosmology - Einstein's, 189, arXiv:astro-ph/0602016.
Belokon, E. T. 1987, Astrophysics, 27, 588
Becker, P. A., Das, S., Le, T. 2008, ApJ, 677, L93
Chatterjee, R., Marscher, A. P., Jorstad, S. G., Olmstead, A. R., McHardy, I. M. et al. 2009, accepted to ApJ, arXiv:0909.2051
Cornwell, T., Fomalont, E.B. 1999, in "Synthesis Imaging in Radio Astronomy II", eds. G. B. Taylor, C. L. Carilli, and R. A. Perley. ASP Conference Series, Vol. 180, (ASP: San Francisco), p. 187.
Daly, R. A., Marscher, A. P. 1988, ApJ, 334, 539
D'Arcangelo, F. D., Marscher, A. P., Jorstad, S. G., Smith, P. S., Larionov, V. et al. 2007, ApJ, 659, L10
Doroshenko, V. T., Sergeev, S. G., Merkulova, N. I., Sergeeva, E. A., Golubinsky et al. 2005, Ap, 48, 304
Doroshenko, V. T., Sergeev, S. G, Efimov, Y. S, Klimanov, S. A. and Nazarov S. V. 2009,AstL, 35, 361
Fomalont, E. B., 1999, in ASPConf.Ser., v.180, synthesis imaging in radio astronomy II, eds. Taylor, G.B., Carilli, C.L., Perley, R.A. (ASP: San Francisco),301
Gómez, J. L., Marti, J. M. A., Marscher, A. P., Ibanez, J. M. A., Marcaide, J. M., 1995, ApJL, 449, L19
Gómez, J. L., Marti, J. M. A., Marscher, A. P., Ibanez, J. M. A., Alberdi, A., 1997, ApJ, 482, L33
Gómez, J. L., Marscher, A. P., Alberdi, A., Jorstad, S. G., Agudo, I., 2001, ApJ, 561, 161
Greene, J. E., & Ho, L. C. 2006, ApJ, 641, L21
Jorstad, S. G., Marscher, A. P., Lister, M. L., Stirling, A. M., Cawthorne, T. V. et al., 2005, AJ, 130, 1418
Kellermann, K. I., Vermeulen, R. C., Zensus, J. A., & Cohen, M. H. 1998, AJ, 115, 1295
Kellermann, K. I., Lister, M. L., Homan, D. C., Vermeulen, R. C., Cohen, M. H et al. 2004, ApJ, 609, 539
Königl, A. 1981, ApJ, 243, 700
Kovalev, Y. Y., Lobanov, A. P., Pushkarev, A. B., Zensus, J. A. 2008, A&A, 483, 759
Lister, M. L. 2003, in ASP Conf. Ser. 300, Radio AStronomy at the Fringe, ed. J.A. Zensus, M.H. Cohen, & E. Ros (San Francisco:ASP),71
Lister, M. L., & Homan, D. C. 2005, AJ, 130, 1389
Lister, M. L., Aller, H. D., Aller, M. F. et al. 2009, AJ, 137, 3718
Lister, M. L., Cohen, M. H., Homan, D. C. et al. 2009, AJ, 138, 1874
Lobanov, A. P., 1996, PhD Thesis, NMIMT, Socorro, USA
Lobanov A. P., 1998, A&A, 330, 79
Lobanov, A. P., 2005, astro-ph/0503225
Lobanov, A.P., Zensus, J.A. 1999, ApJ, 521, 509
Mandal, S., Chakrabarti, S. K. 2008, ApJ, 689, L17
Marshall, K., Ryle, W. T., Miller, H. R., Marscher, A. P., Jorstad, S. G. et al. 2009, ApJ, 696, 601
Marscher A. P. & Gear, W. K. 1985, ApJ, 298, 114
Marscher, A. P., Jorstad, S. G., Gómez, J. L., Aller, M. F.; Teräsranta, H., et al. 2002, Nature, 417, 625
Marscher, A. P.; Jorstad, S. G., D'Arcangelo, F. D., Smith, P. S., Williams, G. G., et al. 2008, Nature, 452, 966
Pearson, T. J., 1997, in ASP Conf. Ser. 180, Synthesis imaging in radio astronomy II, eds. G. B. Taylor, C. R. Carilli, R. A. Perley, 335
Perucho, M., Martí, J. M. 2007, MNRAS, 382, 526
Peterson, B. M., 2002, Advanced Lectures on The Starburst-AGN Connection, eds Aretxaga I., Kunth D. & Mújica R., Singapore World Scientific, 3
Romanova, M. M., Lovelace, R. V. E., 1996, A&AS, 120, 583
Savolainen et al. 2006, A&A, 446, 71
Sergeev, S. G., Doroshenko, V. T., Golubinskiy, Y. V., Merkulova, N. I., & Sergeeva, E. A. 2005, ApJ, 622, 129
Shapovalova, A. I., Burenkov, A. N., Carrasco, L., Chavushyan, V. H., Doroshenko, V. T., et al. 2001, A&A, 376, 775
Schinzel, F., Lobanov, A. P., Zensus, J. A. *(in prep.)*
Soldi, S., Türler, M., Paltani, S., Aller, H. D., Aller, M. F. et al. 2008, A&A, 486, 41
Tyul'bashev, S. A., Chernikov, P. A. 2004, Astronomy Reports, 48, 716
Valtaoja, E. et al. 1999, ApJS, 120, 95
Vlahakis, N. & Königl, A. 2004, ApJ, 605, 656